ARTICLE

Investigating the Graphitization Mechanism of SiO_2 Nanoparticles in Chemical Vapor Deposition

Alicja Bachmatiuk,[†,*] Felix Börrnert,[†] Mandy Grobosch,[†] Franziska Schäffel,[†] Ulrike Wolff,[†] Andrew Scott,[†,‡] Mujtaba Zaka,[§] Jamie H. Warner,[§] Rüdiger Klingeler,[†] Martin Knupfer,[†] Bernd Büchner,[†] and Mark H. Rümmeli[†,‡,*]

[†]IFW Dresden, P.O. Box 270116, 01171 Dresden, Germany, [‡]Technische Universität Dresden, 01062 Dresden, Germany, and [§]Department of Materials, University of Oxford, Parks Rd, Oxford, OX1 3PH, United Kingdom

ABSTRACT The use of SiO_2 as a catalyst for graphitic nanostructures, such as carbon nanotubes and graphene, is a new and rapidly developing catalyst system. A key question is whether carbide phases form in the reaction. We show the formation of SiC from SiO_2 nanoparticles for the synthesis of graphitic carbon nanostructures *via* chemical vapor deposition (CVD) at 900 °C. Our findings point to the carbothermal reduction of SiO_2 in the CVD reaction. The inclusion of triethyl borate apparently accelerates the process and leads to improved yields. The study helps better understand the growth mechanisms at play in carbon nanotube and carbon nanofiber formation when using SiO_2 catalysts.

KEYWORDS: graphene · carbon nanofibers · carbon nanotubes · carbothermal reduction · nonmetal catalysis · SiC

Carbon nanotubes (CNT) and graphene show significant promise in a variety of fields such as high-strength composites,[1,2] electron field emission,[3,4] scanning probe microscopy,[5,6] and molecular electronics.[7−10] Often it is argued that metal catalysts are required for their synthesis, despite the pioneering work by Iijima[11] synthesizing CNT without catalysts. This misconception probably arose because of the sheer success of metal catalysts. Generally it is argued that metal-catalyzed CNT growth occurs through metal−carbon alloys, which can be either in a liquid phase or in a highly mobile solid phase often referred to as "liquidlike". CNT growth then proceeds through the precipitation of carbon through the so-called vapor−liquid−solid (VLS) mechanism.[12] Recently, though, a host of ceramics have been shown to catalyze carbon nanotubes and few layer graphene and so a reconsideration of past growth concepts for CNT is required. The use of SiC for the synthesis of carbon nanotubes[13−15] and graphene[15,16] has been shown. Carbon nanotubes[17−20] and few-layer graphene[20,21] can be obtained through oxide-catalyzed chemical vapor deposition (CVD) routes. Of particular interest is the use of SiO_2 as a catalyst for CNT and graphene formation due to the potential for integration of the latter material into silicon-based technology. The recent success by Huang *et al.*[18] and Liu *et al.*[19] in synthesizing single walled carbon nanotubes from SiO_2 nanoparticles supported on Si/SiO_2 substrates highlights the catalytic graphitization potential of SiO_2 very elegantly. A key question regarding the use of SiO_2 as a graphitization catalyst, as posed by Hirsch,[22] is if SiC forms during the reaction or whether it remains stable. Huang *et al.* conducted X-ray photoemission spectroscopy (XPS) measurements on the wafer and did not find any evidence for SiC. Only SiO_2 was observed, suggesting the SiO_2 particles themselves are the catalytically active species. Other studies also suggest oxides are catalytically active for the graphitization of carbon.[17,21]

In this detailed study we investigate SiO_2 nanoparticles after a CVD reaction. The reaction leads to the formation of carbon nanofibers consisting of stacked graphitic "yarmulke-like caps". The particles at their roots and within them are shown to be SiC. Infrared (IR) and Raman spectroscopy confirm the presence of SiC. SiC can be formed through the carbothermal reduction of silica according to the overall reaction

$$3C + SiO_2 \rightarrow SiC + 2CO \qquad (1)$$

It is generally accepted that SiC forms through intermediate SiO. Thus, the overall

*Addresses correspondence to a.bachmatiuk@ifw-dresden.de, m.ruemmeli@ifw-dresden.de.

Received for review August 3, 2009 and accepted November 5, 2009.

Published online November 12, 2009. 10.1021/nn9009278

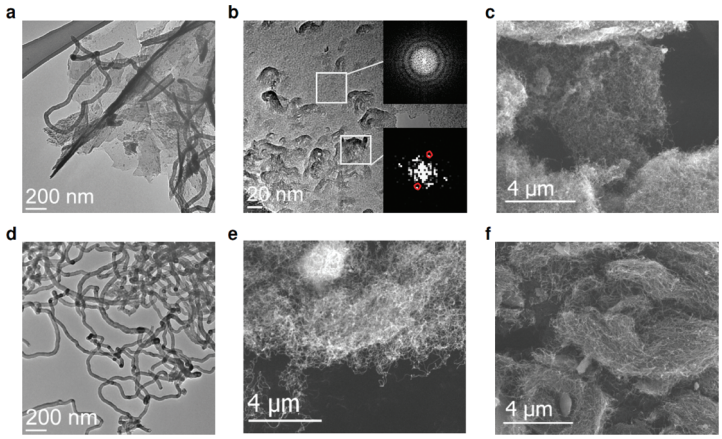

Figure 1. Transmission and scanning electron micrographs providing overviews of the products. (a) TEM showing a few carbon nanofibers and sheets of amorphous carbon produced using a pure ethanol feedstock. (b) Higher magnification TEM providing greater detail on the amorphous carbon sheets. Upper inset: FFT showing rings due to amorphous carbon. Graphitic humps are embedded within as highlighted by the lower inset and show two spots from graphitic carbon. The spots correspond to an interlayer spacing of 3.6 Å. (c) SEM image from a sample prepared using a pristine quartz substrate and an ethanol/triethyl borate mixture as the feedstock. (d and e) TEM and SEM images, respectively, of homogeneous carbon nanofiber formation (ethanol feedstock) from substrates previously used (with a pure ethanol feedstock). (f) SEM showing carbon nanofiber mat formed with ethanol feedstock using a reused substrate after an ethanol/triethyl borate mixture as the feedstock.

reaction can be broken down into two elementary reaction steps:

$$C + SiO_2 \rightarrow SiO + CO \quad (2)$$

$$2C + SiO \rightarrow SiC + CO \quad (3)$$

RESULTS AND DISCUSSION

Commercially available quartz (Saint-Gobain Quartz) serves as both the silica support and provider of SiO_2 nanoparticles in this study. Energy dispersive X-ray spectroscopy (EDX) and X-ray photoemission spectroscopy (XPS) studies confirm the material to consist only of Si and O (see Supporting Information, Figure 1S). The reaction is accomplished using a spray chemical vapor deposition (CVD) system. In the reaction a purpose built spray unit injects the hydrocarbon (ethanol or ethanol/triethyl borate) with argon directly into the reactor. After the reaction a film of soot is seen to have formed on the surface of the quartz substrate. Figure 1 presents scanning electron microscopy (SEM) and transmission electron microscopy (TEM) micrographs of the obtained material.

Images a and b show electron microscopy micrographs of the products produced using pure ethanol as the carbon feedstock. Typically, the surface of the quartz substrate contains only a few carbon nanofibers and is mostly coated by amorphous carbon sheets with small graphitic humps. When using the ethanol/triethyl borate mixture only mats of carbon nanofibers are obtained (panel c). In addition, after the reaction the tube is visibly darker as compared to using a pure ethanol feedstock. To explore the recycling potential of the substrates the supports were heated in air (800 °C for 10 min.) followed by ultrasonication in HCl (1 mol) to remove all carbon species.

These cleaned substrates were then reacted in ethanol (panels d through f). In both cases dense mats of carbon nanofibers were obtained, more so than when using pristine quartz tubes. When using ethanol on the "recycled" substrates no evidence for amorphous carbon sheets was observed (panel d and e). The yield was noticeably higher when using the reused substrate after ethanol/triethyl borate carbon feedstock (panel f). To better comprehend the formation of sp^2 carbon in the reaction more in-depth studies were conducted.

Analysis of the surface morphology of the quartz substrates was accomplished *via* TEM measurements. The studies showed the pristine silica surface to contain amorphous material (Figure 2a), while the samples reacted using ethanol and ethanol/triethyl borate both showed faceted particles with well-defined lattice fringes (e.g., Figure 2b).

A statistical survey of the nanocrystalline particles showed a mean particle size of 2 nm for the ethanol reacted substrate and 3 nm for the ethanol/triethyl borate reacted silica. Fast Fourier transform (FFT) analysis of the particles, as for example shown in the inset of panel b from Figure 2, demonstrates that the crystalline particles are the orthorhombic tridymite phase of SiO_2. X-ray diffraction studies (data not shown) confirm orthorhombic tridymite, and this is in agreement with literature.[24] No borosilicate was observed for samples reacted in ethanol/triethyl borate.

Atomic force microscopy (AFM) investigations (see Supporting Information, Figure 2S) on the silica surfaces before and after the reactions were compared with the surface from the starting material. The starting silica has surface nanostructures between 1 and 4 nm with a mean around 2 nm. After

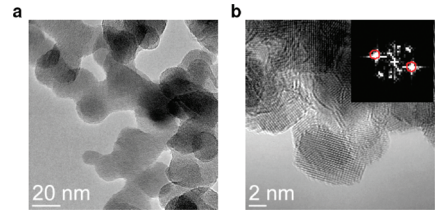

Figure 2. TEM images of the SiO_2 nanoparticles from the substrates surface: (a) pristine (amorphous) substrate, (b) substrate after CVD reaction with pure ethanol, Inset: FFT showing tridymite crystal (400).

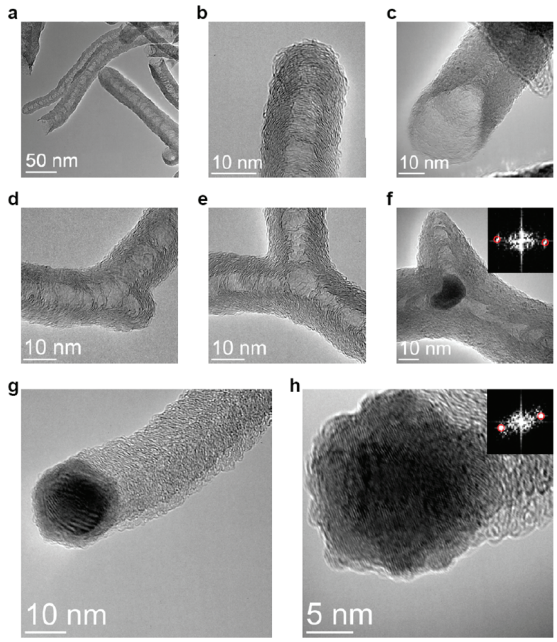

Figure 3. TEM images of the carbon nanostructures synthesized in the CVD experiments from the SiC particles: (a) overview image, (b) carbon nanostructure capped tip, (c) carbon nanostructure open end, (d) branch on a nanofiber, (e) junction, (f) branch with SiC particle residing at the junction. Inset: FFT of the cubic SiC particle (200). (g) SiC particle at the root of a carbon nanofiber, (h) higher magnification of the cubic SiC particle in panel g. Inset: FFT of cubic SiC particle (100).

reacting the tube in pure ethanol (and then cleaned by burning in air followed by ultrasonication in HCl) no difference in the surface roughness is observed. When using the ethanol/triethyl borate mixture the surface roughness was seen to have increased slightly with a mean particle size *ca.* 3 nm. When recycling the silica supports the particle size increased (mean 3−4 nm), and the distributions were bimodal. These values are in excellent agreement with the TEM data. The data suggests that boron lowers the sintering temperature.

Further TEM studies reveal more detailed information on the structure of the as-produced carbon nanofibers. Figure 3 provides an assortment of micrographs of the nanofibers. An overview shows them to contain hollow regions or pockets (panel a). The diameter of the fibers ranged between 10 and 50 nm. Closer inspection indicates the nanostructures comprise stacked hemispheres which are at times incomplete at their poles. The consecutive stacking of these incomplete hemispheres form the observed pockets. The spacing between the layers is (*ca.* 3.6 Å) fully consistent with graphitic interlayer spacing. Two types of ends are obtained. In one, the ends terminate with a hemispherical cap (panel b), while the others are open ended, probably due to separation from catalyst particle (panel c). In addition, a number of the nanofibers have junctions or branches (panels d−f).

Sometimes particles are observed within the structures as is highlighted in panel f in which a particle resides at a Y junction. Furthermore, at times, similar particles are found at the open end of the fiber (panels g and h). Local energy dispersive spectroscopy (EDX) on these particles showed only Si, C, and some oxygen (and traces of Cu from the grid). FFT analysis of the particles shows them to be SiC (*e.g.*, panels f and h).

In the case of samples prepared using ethanol/triethyl borate more detailed spectroscopy was conducted using electron energy loss spectroscopy (EELS) to determine if the carbon nanofibers were B doped. Core level EELS spectra of the samples showed C1s profiles typical for carbon nanotubes (data not shown). The B signals were extremely weak and unclear due to the small B cross-section and instrumental limitations. X-ray photoemission spectroscopy (XPS) is a chemically sensitive technique that better enables the overall B content and the bonding environments to be identified. Hence the samples were subjected to XPS. All samples showed the presence of Si, O, B, and C and confirm no metal impurities are present. Figure 4 shows the XPS spectra for O, C, B, and Si. The O1s peak centered near 533 eV, conforms to that usually obtained for SiO_2. The C1s peak has a maximum at 284.3 eV and a full width at half-maximum of 0.75 eV in good agreement to that reported for multiwalled carbon nanotubes.[24,25] For SiC the C1s peak occurs at 283.5 eV. Since no clear shoulder is observable in the low energy side of the C1s peak, any SiC contribution that may exist is obviously weak relative to the graphitic carbon signal. The B1s peak is broad and lies between 191 and 196 eV and is not fully assigned currently. The

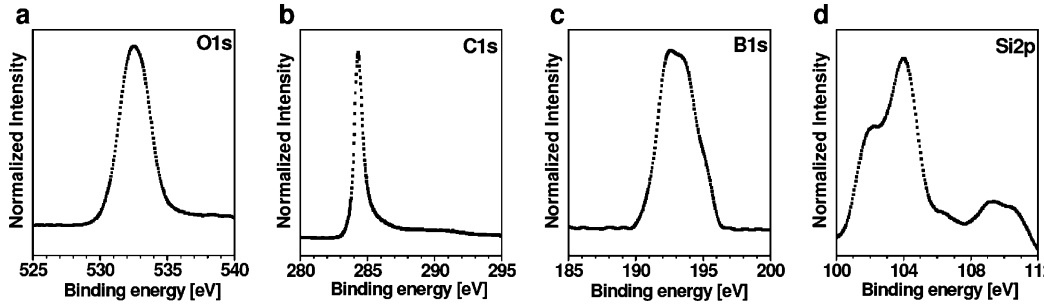

Figure 4. XPS data for core edges from a sample (on its substrate) after a CVD reaction using a ethanol/triethyl borate mixture: (a) O1s edge, (b) C1s edge, (c) B1s edge, (d) Si2p edge.

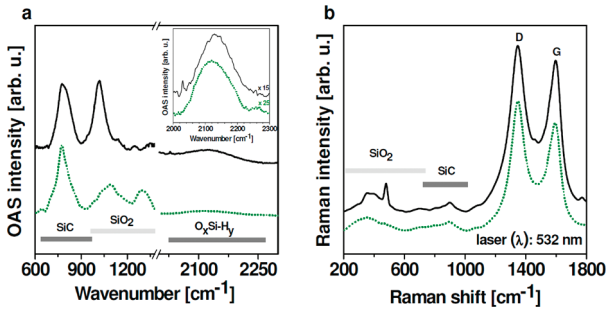

Figure 5. (a) Optical absorption spectra from the samples. Inset: magnification of O_xSi-H_y peaks. (b) Raman spectra (G and D modes from graphite). Solid curve, pure ethanol feedstock; dotted curve, ethanol/triethyl borate mixture.

presence of B_2O_3, H_3BO_3, and B-doped Si occurs between 192 and 194 eV.

Thermodynamic calculations (see Supporting Information, Figure 3S) indicate the presence of B_2O_3. No evidence for pure B (190 eV) is found. In addition, B-doped carbons exhibit a peak at 190 eV. In our studies none was ever observed suggesting that the carbon nanofibers are either not doped or if so, their doping levels are below 0.6%.[26] No peak signals are obtained between 186 and 187 eV showing no B_4C is formed in the process. The Si2p peak is obviously complex. The strongest peak occurs at 104 eV and can be assigned to silica. To the left of this peak a shoulder is clearly discerned, and a deconvolution of it shows a peak occurring close to 101 eV where SiC would be expected. Oxygen depleted silica also leads to peak formation in this region.[27] The origin of the weaker peaks above 105 eV is not clear. However the complex structure of the Si peak does indicate structural changes occur during the carbothermal reduction process. This is further supported by optical absorption (OAS) and Raman spectroscopic studies (Figure 5) on both samples synthesized with pure ethanol and the ethanol/triethyl borate mix. The upper infrared (IR) spectrum in Figure 5 panel a, shows the spectra from the carbon nanostructures prepared using a pure ethanol feedstock.

A broad asymmetric peak is observed between 670 and 900 cm^{-1} and corresponds to SiC.[28] SiO_2 exhibits a strong band between 1000 and 1300 cm^{-1}, where two split longitudinal and transverse optical (LO-TO) pairs arising from Si−O asymmetric stretching are infrared active and are clearly visible in the upper spectrum.[29,30] A sharp peak at 1384 cm^{-1}, also from SiO_2, is present. In the lower spectrum (ethanol/triethyl borate mix) the overall intensity of the SiO_2 features are clearly diminished relative to the SiC peak. Further the SiO_2 peaks between 1000 and 1400 cm^{-1} have broadened, and a stronger feature around 1300 cm^{-1} is now visible. This can be attributed to differences in the LO-TO splitting and is discussed later. The sharp feature at 1384 cm^{-1} has disappeared. Since B is present in the second reaction, it is feasible that silicon borate is also present. Silicon borate should be observable at 640 and 852 cm^{-1}.[31,32] In the lower IR spectrum a minute peak at 640 cm^{-1} and the slightly extended tail on the high frequency side of the SiC peak might be attributed to a Si−O−B response at 852 cm^{-1}. However, similar responses can be obtained from hydrogenated Si at *ca.* 620 and 880 cm^{-1}. Additionally, O_xSi-H species can contribute a signal at *ca.* 880 cm^{-1}. An additional broad peak between 2000 and 2300 cm^{-1} (Figure 5a inset) is attributed to O_xSi-H and O_xSi-H_2 units.[33] These species corroborate the low frequency shoulder of the Si2p XPS data indicating the presence of oxygen-depleted SiO_2. Complementary Raman spectroscopy shows the presence of SiC and SiO_2 in the samples and again, differences between the two feedstocks can be discerned. Typical Raman spectra are presented in Figure 5b. Clear peaks corresponding to SiC (750−1000 cm^{-1}) and SiO_2 (200−800 cm^{-1}) are present. Differences between the two feedstocks for the SiO_2 responses, as found with the IR data, are clearly observable and are attributed to structural differences. At higher frequencies two broad peaks around 1350 and 1600 cm^{-1} are present. The responses indicate sp^2-hybridized carbon through the E2g mode or G band (stretching vibrations in the basal plane of crystalline graphite) and the so-called D band (indicating the level of defects in the graphitic material), respectively.

The formation of sp^2 carbon in this carbothermal reduction route is remarkable for two key reasons. First, SiC formation *via* the solid state carbothermal reduction of silica requires significantly higher temperatures and second the formation of sp^2 carbon on the surface of the SiC is not usually observed (in the carbothermal process). The formation of SiC by the CVD treatment of Si is known at these lower temperatures[34] but again, no observation of sp^2 carbon formation is reported either. In our investigation the XRD and TEM studies show the surface of the amorphous silica to form nanosized tridymite crystals. However, the carbon nanofibers are shown to root to larger silicon carbide particles and at times SiC is found within the fibers. The Raman and OAS spectroscopic data of the surface product confirm the presence of SiC along with some silica. The Raman data also confirm the presence of graphitic carbon as does the XPS data. The XPS data do not clearly show SiC; however, this is probably due to the XPS measurement being conducted with the sample as formed on the silica support in which the total SiC content is then negligible as compared to the SiO_2 content and, more importantly, the SiC is coated by graphitic material essentially blocking its detection. The XPS data do show that the silica support undergoes structural modification in the reac-

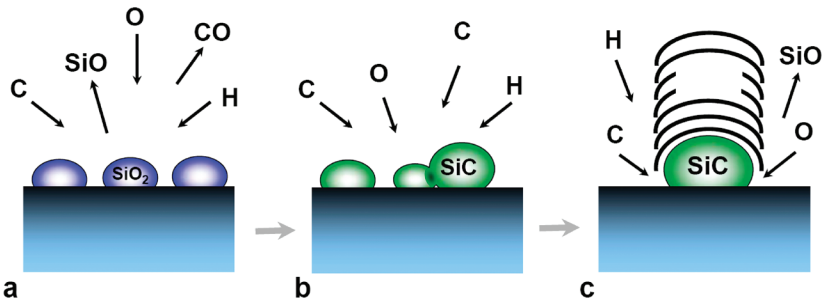

Figure 6. Schematic representation of the steps involved in the carbon nanofiber formation: (a) SiO_2 is reduced to SiC *via* a carbothermal reaction, (b) SiC nanoparticles coalesce, (c) carbon caps form on the surface of the SiC particles through precipitation and/or SiC decomposition.

tion and indicate oxygen depletion in the silica which is further supported by IR spectra (and Raman spectra). In addition, the blue shift of the various SiO_2 LO-TO modes can be attributed to structural changes upon heat treatment.[13,35] The observed changes are fully concomitant with heat treatment and the carbothermal reduction of SiO_2 leading to SiC. The reaction in pure ethanol shows solid carbon species can easily form on the surface; however, very few fibers grow and the graphitic humps embedded within the formed amorphous carbon sheets suggest the amorphous carbon poisons or halts the growth of the fibers. This indicates the source of carbon to the particles is from a gaseous state rather than the solid phase. The inclusion of small quantities of triethyl borate apparently prevents amorphous carbon forming, and high yields of carbon nanofibers are obtained. However, when using a used substrate (recycling) with pure ethanol as the feedstock no amorphous carbon is obtained. This suggests the triethyl borate does not directly prevent amorphous carbon forming but rather it accelerates the crystallization process of the silica indirectly favoring nanofiber (sp^2 carbon) formation over amorphous carbon. The above-discussed differences in the IR data from both feedstocks would seem to support this argument. The TEM studies on the fibers themselves and the SiC particles provide further insight into aspects of their growth. The SiC particles tend not to be faceted, but exhibit smooth curved surfaces. Particles found within the nanostructures at kinks are curved in a manner adopting the curvature of the bend in which they reside. They appear to suggest they had liquidlike character during the reaction. The melting point for bulk SiC is just above 2700 °C which is significantly higher than our reaction temperature of 900 °C. However, nanosized particles are known to have reduced melting points and further the possible presence of other species (e.g., hydrogen and/or boron) might further reduce the eutectic temperature. In addition, the formation of the graphitic caps forming the carbon nanofiber could very easily be explained through a precipitation mechanism similar to that in the vapor−liquid−solid mechanism described by Baker[35] for carbon nanotubes/nanofibers grown from conventional metal catalysts. An alternative or parallel mechanism may also be operative. It is well-known that in forming carbon nanotubes or graphene from the decomposition of SiC at elevated temperatures in vacuum trace amounts of oxygen are required to maintain the reaction.[13] The reaction requires CO and occurs as follows:

$$SiC + CO \rightarrow SiO + 2C \quad (4)$$

The reduction of SiO_2 provides a source of CO. Further, our thermodynamic calculations (Supporting Information, Figure 3S) show CO is a product from the hydrocarbon feedstock(s) decomposition. However, if reaction 4 was significant one would anticipate the fiber diameters to decrease during growth as the catalyst particle looses mass through Si removal. Our data show the diameters of the nanostructures are uniform. In addition, the diameter of the catalyst particles at the root of a fiber matches that of the fiber itself. This suggests reaction 4 is unlikely. Hence, the likely mechanism is the dissolution of carbon from the vapor phase into the particles followed by precipitation from a liquid or liquidlike particle, *viz.*, the VLS mechanism as found with metal catalysts is probably occurring in this reaction too.

In addition, the data clearly show that the coalescence of SiC particles occurs during the reaction. This is supported by the significantly larger size (an order of magnitude) of the SiC particles to that of the crystalline silica nanoparticles. The coalescence of the SiC particles can explain the large number of Y junctions and branches on the carbon nanostructures; SiC particles moving on the substrate surface can come into contact with another SiC particle which is already growing a carbon nanostructure. One can envisage that the coalescing particle may also start to grow a nanofiber and in doing so form a branch or Y junction. The large number of Y junctions and branches suggests the SiC particles are very mobile during the reaction.

Figure 6 presents a schematic overview illustrating the various steps in which the SiO_2 is reduced *via* a carbothermal reaction forming SiC. The newly formed SiC particles begin coalescing and then the carbon nanofibers grow.

CONCLUSION

Our findings show that SiO_2 nanoparticles exposed to a CVD reaction are reduced to SiC through a carbothermal reduction route. The formation of carbon nanofibers consisting of stacked yarmulke

and the particles shape suggest bulk carbon diffusion of carbon occurs. The inclusion of triethyl borate apparently accelerates the restructuring process and leads to improved yields of carbon nanofibers free of amorphous carbon. The optimization of the technique is attractive for the synthesis of both carbon nanotubes and graphene suitable for integration within silicon technology.

EXPERIMENTAL SECTION

The CVD process temperature was 900 °C and the reaction time was 30 min. The obtained products were studied using aberration-corrected transmission electron microscopy (TEM, FEI Titan^3 operated at 80 kV). In addition, scanning electron microscopy (SEM, FEI Nova-Nanosem) and atomic force microscopy (AFM, Dimension 3100 Veeco) were used to characterize samples further. IR optical absorption spectroscopy was obtained using a Bruker 113 Fourier transform spectrometer, while Raman spectra were measured using Thermo Scientific DXR SmartRaman spectrometer (excitation laser $\lambda = 532$ nm). Photoemission X-ray spectroscopy (XPS) was measured with a PHI 5600 spectrometer with photon energy 1486.6 eV from a monochromatized Al Kα source. The total energy resolution of the spectrometer was determined by analyzing the width of the Au Fermi edge to be about 350 meV. The binding energy scale was aligned by measuring the Fermi edge (0 eV) and the $Au4_{7/2}$ emission feature (84.0 eV) of a polycrystalline gold substrate. X-ray diffraction measurements were performed using Philips X'pert diffractometer with a cobalt lamp. Electron energy loss spectroscopy was conducted on a purpose-built high-resolution^{23} spectrometer where the energy resolution was set to 200 meV and momentum resolution was 0.1 Å^{-1}.

Acknowledgment. The research was supported in part by the European Network CARBIO, Contract MRTN-CT-2006-035616. F.S. acknowledges funding from the Cusanuswerk. A.S. thanks the EU for support *via* its ERASMUS program. We are grateful to S. Leger, R. Schönfelder, M. Ulbrich, and R. Hübel for technical support.

Supporting Information Available: EDX spectra, AFM measurements, and thermodynamics calculations. This material is available free of charge *via* the Internet at http://pubs.acs.org.

REFERENCES AND NOTES

1. Ma, W.; Liu, L.; Zhang, Z.; Yang, R.; Liu, G.; Zhang, T.; An, X.; Yi, X.; Ren, Y.; Niu, Z.; *et al.* High-Strength Composite Fibers: Realizing True Potential of Carbon Nanotubes in Polymer Matrix through Continuous Reticulate Architecture and Molecular Level Couplings. *Nano Lett.* **2009**, *9*, 2855−2861.
2. Stankovich, S.; Dikin, D. A.; Dommett, G. H. B.; Kohlhaas, K. M.; Zimney, E. J.; Stach, E. A.; Piner, R. D.; Nguyen, S. T.; Ruoff, R. S. Graphene-Based Composite Materials. *Nature* **2006**, *442*, 282–286.
3. de Heer, W. A.; Chatelain, A.; Ugarte, D. A. A Carbon Nanotube Field-Emission Electron Source. *Science* **1995**, *270*, 1179–1180.
4. Tans, S. J.; Verschueren, A.; Dekker, C. Room-Temperature Transistor Based on a Single Carbon Nanotube. *Nature* **1998**, *393*, 49–52.
5. Dai, H. J.; Hafner, J. H.; Rinzler, A. G.; Colbert, D. T.; Smalley, R. E. Nanotubes as Nanoprobes in Scanning Probe Microscopy. *Nature* **1996**, *384*, 147–150.
6. Hafner, J.; Cheung, C.; Lieber, C. Growth of Nanotubes for Probe Microscopy Tips. *Nature* **1999**, *398*, 761–762.
7. Martel, R.; Schmidt, T.; Shea, H. R.; Hertel, T.; Avarious, P. Single- and Multi-Wall Carbon Nanotube Field-Effect Transistors. *Appl. Phys. Lett.* **1998**, *73*, 2447–2449.
8. Soh, H.; Morpungo, A.; Kong, J.; Marcus, C.; Quante, C.; Dai, H. Integrated Nanotube Circuits: Controlled Growth and Ohmic Contacting of Single-Walled Carbon Nanotubes. *Appl. Phys. Lett.* **1999**, *75*, 627.
9. Kong, J.; Franklin, N. R.; Zhou, C.; Chapline, M. G.; Peng, S.; Cho, K.; Dai, H. Nanotube Molecular Wires as Chemical Sensors. *Science* **2000**, *287*, 622–625.
10. Postma, H. W. C.; Teepen, T.; Yao, Z.; Grifoni, M.; Dekker, C. Carbon Nanotube Single-Electron Transistors at Room Temperature. *Science* **2001**, *293*, 76–79.
11. Iijima, S. Helical Microtubules of Graphitic Carbon. *Nature* **1991**, *354*, 56–58.
12. Wagner, R. S.; Ellis, W. C. Vapor−Liquid−Solid Mechanism of Single Crystal Growth. *Appl. Phys. Lett.* **1964**, *4*, 89–90.
13. Kusunoki, M.; Suzuki, T.; Hirayama, T.; Shibata, N. A Formation Mechanism of Carbon Nanotube Films on SiC (0001). *Appl. Phys. Lett.* **2000**, *77*, 531–533.
14. Kusunoki, M.; Suzuki, T.; Hirayama, T.; Shibata, N. A. Aligned Carbon Nanotube Films on SiC (0001) Wafers. *Phys. B* **2002**, *323*, 296–298.
15. Takagi, D.; Hibino, H.; Suzuki, S.; Kobayashi, Y.; Homma, Y. Carbon Nanotube Growth from Semiconductor Nanoparticles. *Nano Lett.* **2007**, *7*, 2272–2275.
16. Ohta, T.; El Gabaly, F.; Bostwick, A.; McChesney, J. L.; Emtsev, K. V.; Schmid, A. K.; Seyller, T.; Horn, K.; Rotenberg, E. Morphology of Graphene Thin Film Growth on SiC (0001). *New J. Phys.* **2008**, *10*, 023034.
17. Rümmeli, M. H.; Schäffel, F.; Kramberger, C.; Gemming, T.; Bachmatiuk, A.; Kalenczuk, R. J.; Büchner, B.; Pichler, T. Oxide-Driven Carbon Nanotube Growth in Supported Catalyst CVD. *J. Am. Chem. Soc.* **2007**, *129*, 15772–15773.
18. Huang, S.; Cai, Q.; Chen, J.; Quian, Y.; Zhang, L. Metal-Catalyst-Free Growth of Single-Walled Carbon Nanotubes on Substrates. *J. Am. Chem. Soc.* **2009**, *131*, 2094–2095.
19. Liu, B.; Ren, W.; Gao, L.; Li, S.; Pei, S.; Liu, C.; Jiang, C.; Cheng, H.-M. Metal-Catalyst-Free Growth of Single-Walled Carbon Nanotubes. *J. Am. Chem. Soc.* **2009**, *131*, 2082–2083.
20. Rümmeli, M. H.; Schaeffel, F.; de los, Arcos, T.; Haberer, D.; Bachmatiuk, A.; Kramberger, C.; Ayala, P.; Borowiak-Palne, E.; Adebimpe, D.; Gemming, T.; *et al.* On the Graphitization Role of Oxide Supports in Carbon Nanotube CVD Synthesis. *Phys. Status Solidi B* **2008**, *245*, 1939–1942.
21. Rümmeli, M. H.; Kramberger, C.; Grüneis, A.; Ayala, A.; Gemming, T.; Büchner, B.; Pichler, T. On the Graphitization Nature of Oxides for the Formation of Carbon Nanostructures. *Chem. Mater.* **2007**, *19*, 4105–4107.
22. Hirsch, A. Growth of Single-Walled Carbon Nanotubes without a Metal Catalyst—A Suprising Discovery. *Angew. Chem., Int. Ed.* **2009**, *48*, 2–4.
23. Fink, J. Recent Developments in Energy-Loss Spectroscopy. *Adv. Electron. Electron Phys.* **1989**, *75*, 121–232.
24. Hlavac, J. *Glass Science and Technology, The Technology of Glass and Ceramics*; Elsevier: Czechoslovakia, 1983; p 12−13.
25. Lim, S. H.; Elim, H. I.; Gao, X. Y.; Wee, A. T. S.; Ji, W.; Lee, J. Y.; Lin, J. Electronic and Optical Properties of Nitrogen-Doped Multiwalled Carbon Nanotubes. *Phys. Rev. B* **2006**, *73*, 045402-1−045402-6.
26. Bystrzejewski, M.; Bachmatiuk, A.; Thomas, J.; Ayala, P.; Hübers, H.-W.; Gemming, T.; Borowiak-Palen, E.; Pichler, T.; Kalenczuk, R. J.; Büchner, B.; *et al.* Boron-Doped Carbon Nanotubes *via* Ceramic Catalysts. *Rapid Res. Lett.* **2009**, *3*, 193–195.
27. Hao, X. J.; Cho, E.-C.; Flynn, C.; Shen, Y. S.; Conibeer, G.; Green, M. A. Effects of Boron Doping on the Structural and Optical Properties of Silicon Nanocrystals in a Silicon Dioxide Matrix. *Nanotechnology* **2008**, *19*, 424019.

28. Rümmeli, M. H.; Adebimpe, D. B.; Borowiak-Palen, E.; Gemming, T.; Ayala, P.; Ioannides, N.; Pichler, T.; Huczko, A.; Cudzilo, S.; Knupfer, M.; *et al*. Hydrogen Activated Axial Interconversion in SiC Nanowires. *J. Solid State Chem.* **2009**, *182*, 602–607.
29. Kamitos, E. I.; Patsis, A. P.; Kordas, G. Infrared-Reflectance Spectra of Heat-Treated Sol−Gel-Derived Silica. *Phys. Rev. B* **1993**, *48*, 12499–12505.
30. Kirk, C. T. Quantitative Analysis of the Effect of Disorder-Induced Mode Coupling on Infrared Absorption in Silica. *Phys. Rev. B* **1998**, *38*, 1255–1273.
31. Parashar, V. K.; Orhan, J.-B.; Sayah, A.; Cantoni, M.; Gijs, M. A. M. Borosilicate Nanoparticles Prepared by Exothermic Phase Separation. *Nat. Nanotechnol.* **2008**, *3*, 589–594.
32. Sigoli, F. A.; Kawano, Y.; Davolos, M. R.; Jafelicci, M. Phase Separation in Pyrex Glass by Hydrothermal Treatment: Evidence from Micro-Raman Spectroscopy. *J. Non-Cryst. Solids* **2001**, *284*, 49–54.
33. Higo, M.; Nishino, K.; Kamata, S. Characterization of Evaporated Si and SiO Films by Inelastic Electron Tunneling Spectroscopy. *J. Phys. Chem.* **1992**, *96*, 1848–1854.
34. Khan, I. H.; Summergrad, R. N. The Growth of Single-Crystal Films of Cubic Silicon Carbide on Silicon. *Appl. Phys. Lett.* **1967**, *11*, 12–13.
35. Baker, R. T. K.; Harris, P. S. *Formation of Filamentous Carbon in Chemistry and Physics of Carbon*; Marcel Dekker: New York, 1978.